Gut Pathogens

RESEARCH

Open Access

Relative abundance of a gut-derived *Lancefieldella parvula* strain is associated with severe inflammation in IBD

Sasanka Weerasingha[1,2], Austin Yan[1,2], James Butcher[1,2], David R. Mack[3,4] and Alain Stintzi[1,2,5*]

Abstract

Background *Lancefieldella parvula* (previously known as *Atopobium parvulum*) has been associated with inflammatory bowel disease (IBD); however, prior in vivo studies relied on an oral-derived reference strain rather than intestinal clinical isolates, limiting interpretation of its role in gut inflammation. To address this gap, we isolated a clinical strain of *L. parvula* (designated *L. parvula* TI19E08) from a mucosal luminal aspirate of an ulcerative colitis (UC) participant. We developed a strain-specific quantitative PCR assay to quantify its abundance across anatomical sites in treatment-naïve pediatric IBD participant (UC and Crohn's disease (CD)) and examined its relationship with site-specific endoscopic inflammation severity.

Results We demonstrated that the relative abundance of *L. parvula* TI19E08 increased with increasing local inflammation severity. In UC, both strain-specific and total *L. parvula* levels were strongly correlated with inflammation severity, particularly in the proximal colon. In CD patients, strain-level associations were most pronounced in the terminal ileum, which is consistent with the disease distribution.

Conclusion This study characterizes an intestinal *L. parvula* isolate and demonstrates that strain-level expansion correlates with disease severity across IBD subtypes and anatomical regions. These findings identify *L. parvula* TI19E08 as a candidate mucosal marker of inflammation severity in IBD patients.

Keywords Inflammatory bowel disease, *Lancefieldella parvula*, Gut microbiome, Inflammation severity, Mucosal biomarker

Background

Inflammatory bowel disease (IBD) represents a group of complex, multifactorial disorders that significantly impact global health, with increasing incidence rates worldwide [1]. IBD encompasses two primary chronic inflammatory conditions of the gastrointestinal tract: Crohn's disease (CD) and ulcerative colitis (UC) [2]. While both diseases involve dysregulated immune responses and gut microbiome alterations, they differ significantly in their anatomical distribution, histological characteristics, and clinical presentations [3]. CD can affect any part of the gastrointestinal tract in a

*Correspondence:
Alain Stintzi
astintzi@uottawa.ca
[1]School of Pharmaceutical Sciences, Faculty of Medicine, University of Ottawa, Ottawa, ON, Canada
[2]Department of Biochemistry, Microbiology and Immunology, Faculty of Medicine, University of Ottawa, Ottawa, ON, Canada
[3]Department of Pediatrics, Faculty of Medicine, University of Ottawa, Ottawa K1H 8M5, ON, Canada
[4]Inflammatory Bowel Disease Centre and CHEO Research Institute, Children's Hospital of Eastern Ontario, Ottawa K1H 8L1, ON, Canada
[5]Université de Strasbourg, CNRS, IPHC UMR7178, Strasbourg, France

© The Author(s) 2026. **Open Access** This article is licensed under a Creative Commons Attribution-NonCommercial-NoDerivatives 4.0 International License, which permits any non-commercial use, sharing, distribution and reproduction in any medium or format, as long as you give appropriate credit to the original author(s) and the source, provide a link to the Creative Commons licence, and indicate if you modified the licensed material. You do not have permission under this licence to share adapted material derived from this article or parts of it. The images or other third party material in this article are included in the article's Creative Commons licence, unless indicated otherwise in a credit line to the material. If material is not included in the article's Creative Commons licence and your intended use is not permitted by statutory regulation or exceeds the permitted use, you will need to obtain permission directly from the copyright holder. To view a copy of this licence, visit http://creativecommons.org/licenses/by-nc-nd/4.0/.

discontinuous, transmural pattern [4], whereas UC is characterized by continuous, mucosal inflammation limited to the colon and rectum [5]. Pathophysiological differences between the two disease subtypes have important implications for disease monitoring, with CD severity often clinically assessed via the pediatric Crohn's disease activity index (PCDAI) [6] or its variations [7] and UC being assessed via different scoring systems, such as the pediatric ulcerative colitis activity index (PUCAI) [8].

Lancefieldella parvula is a nonmotile, obligately anaerobic, gram-positive bacterium belonging to the phylum Actinomycetota (Actinobacteria) [9]. *L. parvula* was initially identified in human oral microbiomes [10] but has subsequently been detected in the human duodenal mucosal microbiome [11] and human fecal samples [12, 13] at very low abundance. *L. parvula* has been associated with various human pathologies, including halitosis [14], colorectal cancer [15–18] and IBD [19].

Previous research has demonstrated that the relative abundance of *L. parvula* is increased in mucosal luminal aspirates collected from the proximal colon of pediatric participants with CD, but several key questions regarding the potential role of *L. parvula* in IBD remain unresolved [19]. First, *L. parvula* levels were profiled in only one gastrointestinal region, the proximal colon, and an overall, rather than a site specific, metric of disease severity was employed to correlate bacteria levels with disease severity [19]. Second, detailed assessments of overall *L. parvula* abundance were only conducted in CD patients, limiting insight into its potential relevance across IBD subtypes [19]. Finally, much of the prior work has relied on *L. parvula* type strain (ATCC 33793 = DSM 20469) [9], originally isolated from the oral microbiome (gingival crevices of the human oral cavity), including for quantitative PCR (qPCR) primer design and subsequent in vivo validation [19]. Given the potential for strain-level heterogeneity and niche-specific adaptation [20], these limitations restrict the interpretation of the role of *L. parvula* in intestinal inflammation.

Table 1 Basic genomic features of *L. parvula* TI19E08

Parameter	Value
Genome size (bp)	1,582,852
No. of contigs	1
Largest contig (bp)	1,582,852
N50	1,582,852
GC (%)	48.17
Mean coverage	4,433
BUSCO completeness (%)	98.8
Coding sequences (CDSs)	1,342
Transfer RNAs (tRNAs)	45
Noncoding rRNAs (ncRNAs)	3
Ribosomal RNAs (rRNAs)	6
Pseudogenes	3
SRA accession number	SRR37363788
BioProject	PRJNA1428198
BioSample	SAMN55948402
GenBank accession number	JBVNCW000000000

To further characterize the in vivo role of *L. parvula* in IBD, we isolated a clinical strain of *L. parvula* (named TI19E08), developed a strain-specific qPCR assay to quantify the relative abundance of this strain from the terminal ileum to the distal colon in both CD and UC participants, and assessed *L. parvula* levels via disease-specific regional metrics of mucosal inflammation. Our findings demonstrate that the relative abundance of this strain increases with increasing inflammation severity in both UC and CD, suggesting that *L. parvula* TI19E08 could be a potential prognostic biomarker of inflammation severity in IBD and supporting further investigation into its role in disease pathogenesis 1.

Methods

Ethics statement

The collection of samples from pediatric IBD participants was approved by the Research Ethics Board of the Children's Hospital of Eastern Ontario (CHEO, #09/37X) in Ottawa, Canada. Informed written consent/assent was obtained from parents and/or participants.

Sample collection

The participants followed the standard colonoscopy preparation protocol the day before the colonoscopy. The exclusion criteria for participants were diabetes mellitus; body mass index (BMI) at or above the 95th percentile for age; infectious gastroenteritis within two months prior to colonoscopy; antibiotic, prebiotic, or probiotic use within the last 4 weeks before colonoscopy; or irritable bowel syndrome.

During endoscopy, mucosal luminal interface (MLI) aspirate samples were collected by a physician from the terminal ileum (TI), proximal colon (PC) and distal colon (DC), as previously described [21]. Briefly, mucosa from these sites was flushed with sterile water to dislodge the adherent mucus layer, and the intestinal wash containing the mucus, microbiota and intestinal cells was aspirated through the colonoscope into a sterile container. These samples were immediately placed on ice, transferred to the laboratory and stored at −80 °C until DNA extraction. In addition, 1 mL MLI aliquots from each sampled region were cryopreserved for subsequent strain isolations by adding 1 mL 50% glycerol + 0.1% cysteine and storing the 2 mL solutions at −80 °C.

Participant selection

A total of 80 children newly diagnosed with IBD (38 with UC and 42 with CD) were selected retrospectively

Table 2 Statistics for study participants

Diagnosis	Number of participants	Sex(F/M)	Average age (years)	Location	Mayo Score/SES-CD score	Total sample number by location
UC	38	19/19	13.9 ± 3.1	TI	Grade 0: Normal or inactive disease: 13	13
				PC	Grade 0: Normal or inactive disease: 5	24
					Grade 1: Mild disease: 5	
					Grade 2: Moderate disease: 8	
					Grade 3: Severe disease: 6	
				DC	Grade 0: Normal or inactive disease: 5	20
					Grade 1: Mild disease: 3	
					Grade 2: Moderate disease: 7	
					Grade 3: Severe disease: 5	
CD	42	15/27	13.3 ± 2.8	TI	SES-CD Ileum score 0: 7	27
					SES-CD Ileum score 1–3: 4	
					SES-CD Ileum score 4–6: 6	
					SES-CD Ileum score 7–9: 5	
					SES-CD Ileum score 10–12: 5	
				PC	SES-CD right score 0: 5	22
					SES-CD right score 1–3: 5	
					SES-CD right score 4–6: 5	
					SES-CD right score 7–9: 5	
					SES-CD right score 10–12: 2	
				DC	SES-CD left score 0: 5	20
					SES-CD left score 1–3: 5	
					SES-CD left score 4–6: 5	
					SES-CD left score 7–9: 5	

Table 3 Endoscopic indices used to classify inflammation severity

Disease/index	Score/group	Category	Description
UC: Mayo score	Grade 0	Normal/inactive disease	
	Grade 1	Mild disease	erythema, decreased vascular pattern, mild friability
	Grade 2	Moderate disease	marked erythema, absent vascular pattern, friability, erosions
	Grade 3	Severe disease	spontaneous bleeding, ulceration
CD: SES-CD (Segment score*)	Group 1	-	left/right/ileum score = 0
	Group 2	-	left/right/ileum score = 1–3
	Group 3	-	left/right/ileum score = 4–6
	Group 4	-	left/right/ileum score = 7–9
	Group 5	-	left/right/ileum score = 10–12

*Per-segment SES-CD for the distal colon (left), proximal colon (right) and terminal ileum (ileum)

for analysis. Participants were selected on the basis of inflammation severity, with a minimum of 5 samples per severity grade/group. The sample distribution was balanced across the inflammation categories and sample locations where feasible. Owing to limited sample availability, some severity groups contained fewer than 5 samples or no samples. In particular, our cohort did not contain any UC participants with 'backwash ileitis' and thus all TI samples from these participants were non-inflamed. Detailed statistics for these participants are summarized in Table 2. All participants were newly diagnosed with IBD during the diagnostic colonoscopy and had not received any IBD-specific treatments prior to sample collection.

Mucosal inflammation severity was assessed using disease-specific endoscopic scoring systems: the Mayo endoscopy sub-score (grade 0 to grade 3) for UC [22] and the Simple Endoscopic Score for CD (SES-CD) [23]. The SES-CD scores for the distal colon (left score), proximal colon (right score) and terminal ileum (ileum score) were binned into five ordinal groups for analysis: group 1 (SES = 0), group 2 (1–3), group 3 (4–6), group 4 (7–9) and group 5 (10–12), representing increasing inflammation severity (Table 3).

Metagenomic DNA extraction

Metagenomic DNA extraction was performed as previously described [19]. Briefly, DNA was extracted using the Fast DNA Spin Kit and a FastPrep 5G. The extracted DNA was quantified using a Qubit fluorometer, normalized to 5 ng/µL and stored at −20 °C until further testing.

Growth media

An *Lancefieldella* (*Atopobium)*-specific medium [24] (ASM) was used to isolate and maintain the *L. parvula* strains used in this study. ASM was prepared by supplementing fastidious anaerobe broth (FAB) for broth cultures or fastidious anaerobe agar (FAA) for solid cultures, with 0.02% (v/v) Tween 80 and 10% (v/v) sterile-filtered rabbit serum (Fisher Scientific, 16120099). Rabbit serum was added aseptically after autoclaving, either immediately before agar plates were poured or just prior to inoculation for liquid cultures. For broth cultures, biphasic flasks were prepared with a thin agar layer (approximately 3 mm) using 6 mL of agar and overlaid with 6 mL of broth medium in culture flasks (Fisher Scientific, 10–126–28). ASM agar plates/biphasic flasks were stored at 4 °C until use. One day before culturing, the culture media were transferred to an anaerobic chamber (BactronEZ anaerobic chamber) for prereduction.

Bacterial strains and growth conditions

L. parvula (ATCC 33793) was obtained from the American Type Culture Collection (ATCC). A clinical strain of *L. parvula* was isolated from the MLI of a UC participant during the study, described below. These bacterial strains were handled and cultured in an anaerobic chamber. The bacterial cells were stored at −80 °C in sterile, prereduced 70% glycerol in phosphate-buffered saline (PBS) supplemented with 0.1% L-cysteine. When needed, the bacteria were revived from frozen glycerol stocks by streaking onto prereduced ASM agar medium.

Bacterial isolation, identification, and growth curve

To obtain clinical, intestinal-derived isolates of *L. parvula*, we identified a patient MLI sample (TI19) that contained a high relative abundance of *L. parvula* on the basis of shotgun metagenomic sequencing. This MLI sample was obtained from the TI of an individual with UC. The glycerol-preserved MLI sample from this participant was streaked onto prereduced ASM agar plates and incubated for 48 h at 37 °C under anaerobic conditions. Distinct colonies were picked and suspended in 10 µL ddH_2O, heated at 95 °C and used as input for direct colony PCR for three separate reactions via Taq polymerase (Thermo Fisher) and three sets of primers: *L. parvula* primers previously described by Mottawea et al. [19]. Newly designed *L. parvula* primers were designed on the basis of shotgun metagenomic sequencing of TI19, and the BOX A1R primer [25] was used for molecular fingerprinting to dereplicate strains (Table 4). The PCR conditions for the *L. parvula* reactions were as follows: 94 °C for 3 min; 94 °C for 45 s, 60 °C for 30 s, and 72 °C for 45 s for 30 cycles; and 72 °C for 10 min. The BOX PCR program was 95 °C for 7 min; 95 °C for 30 s, 53 °C for 60 s, and 65 °C for 8 min for 30 cycles; and 72 °C for 16 min. Isolates with possible amplification of the *L. parvula* amplicon underwent further subculture, DNA extraction (Fast DNA Spin Kit in combination with a FastPrep-5G instrument as described above) and full-length 16 S rRNA gene PCR for isolate identification to confirm the isolation of *L. parvula*, which led to the isolation of strain TI19E08. During the course of this process, we also isolated a clinical strain of *L. rimae* TI19B36 from the same participant. This strain was used to assess the specificity of our final qPCR primer set.

A bacterial growth curve was generated to characterize TI19E08 growth kinetics. Bacteria from frozen stock cultures were streaked onto ASM agar plates and incubated overnight at 37 °C under anaerobic conditions. A single colony was subsequently transferred to ASM broth in a biphasic culture flask and incubated overnight. The following morning, this culture was transferred to a fresh

Table 4 Primers used in the study

Target bacterium	Primer ID	Sequence	Reference
L. parvula TI19E08	AtP1F AtP1R	5′-CGGCGGTAAAAGAGGTTAGAGCG-3′ 5′-CCAGTTGGGCGATCCTATAAAAACA-3′	This study
L. parvula TI19	YAN_AP1F YAN_AP2R	5′-CAAGATCAGCCTGACGCTGGTCAAAC-3′ 5′-GCAACTCGTCAGACAAGCCCTATCTC-3′	This study
L. parvula spp.	Aparv-711 F Aparv-881R	5′- GGGGAGTATTTCTTCCGTGCCG – 3′ 5′- CTTCACCTAAATGTCAAGCCCTGG – 3′	(Mottawea et al. 2016) [19]
Total Bacteria	UniF UniR	5′-GTGSTGCAYGGYYGTCGTCA-3′ 5′-ACGTCRTCCMCNCCTTCCTC-3′	Fuller et al. 2007 [33]
BOX PCR Fingerprinting	BOX A1R	5′-CTACGGCAAGGCGACGCTGACG-3′	Alex van & Peter Hermans [25]
16 S rRNA	BACT 8 F 1391R	5′-AGAGTTTGATCCTGGCTCAG-3′ 5′-GACGGGCGGTGWGTRCA-3′	Edwards et al. 1989 [42]

biphasic flask at a starting optical density at 600 nm (OD_{600}) of 0.1 and incubated at 37 °C under anaerobic conditions. During incubation, 250 µL aliquots were collected, and the optical density was measured using a microplate reader. Growth was monitored over 21 h to establish a growth curve (Supplementary Fig. 1).

Whole genome sequencing and genome analysis

Genomic DNA from *L. parvula* TI19E08 was extracted using the Quick-DNA HMW Kit (Cederlane, D6060). The purity of the extracted genomic DNA was evaluated with a Nanodrop spectrophotometer, and the concentration was determined using a Qubit fluorometer with a Qubit High Sensitivity Assay Kit following the manufacturer's protocol. The size of the DNA fragments was verified by gel electrophoresis on a 0.5% agarose gel, with the GeneRuler High Range DNA Ladder (Thermo Fisher Scientific, SM1353) used as a molecular weight marker.

Genome sequencing was conducted with Oxford Nanopore technology according to the manufacturer's protocols. Briefly, unsheared and non-size-selected DNA was used to generate tagmentation libraries as four barcoded technical replicates using a Rapid Barcoding Kit (ONT, SQK-RBK114-24) and sequenced on a MinION using a single flow cell (ONT, FLO-MIN114) for 72 h. In addition, short-read sequencing data for assembly polishing were generated using an Ion Torrent PGM with an Ion 318 chip. Libraries were prepared from genomic DNA extracted using the FastDNA protocol described above via Ion Xpress Plus Fragment Library Kit according to the manufacturer's instructions. Raw reads associated with these experiments have been deposited to NCBI SRA under accession PRJNA1428198.

Subsequent bioinformatic analyses used the default parameters for each program unless otherwise noted. The raw reads were base-called, adapter-trimmed and demultiplexed using Dorado (v0.9.2, https://github.com/nanoporetech/dorado) with the super accuracy (sup) model to maximize basecalling accuracy. Low-quality reads (Q score < 8) were discarded. Reads from the four barcoded replicates were concentrated prior to assembly, yielding a total of 1,190,922 reads (N50 = 16,831 bp; total bases = 7.2 Gbp) for *de novo* assembly with Flye (v2.9.5-b1801) [26]. The draft assembly was polished using short-read Ion Torrent sequencing data with a total of 5,470,576 reads (read length range 25–613 bp; total bases = 1.3 Gbp), corresponding to approximately 867x coverage of the genome. The reads were aligned to the draft assembly using BWA-MEM (v0.7.19) [27], and polishing was performed with PolyPolish (v0.6.1) [28]. Assembly quality was evaluated with QUAST (v5.3.0) [29], and genome completeness was assessed with BUSCO (v6.0.0) [30]. The genome assembly has been deposited in NCBI under accession number JBVNCW000000000. Phylogenetic analysis was performed using whole-genome taxonomy-based analysis via the Type (Strain) Genome Server (TYGS) [31], and the resulting tree was visualized using iTOL (v7.4.2) [32] (Fig. 1).

Primer design

For the abundance analysis, three different primer sets were used (Table 4). A strain-specific primer set (AtP1F/R) was designed to target *L. parvula* TI19E08,

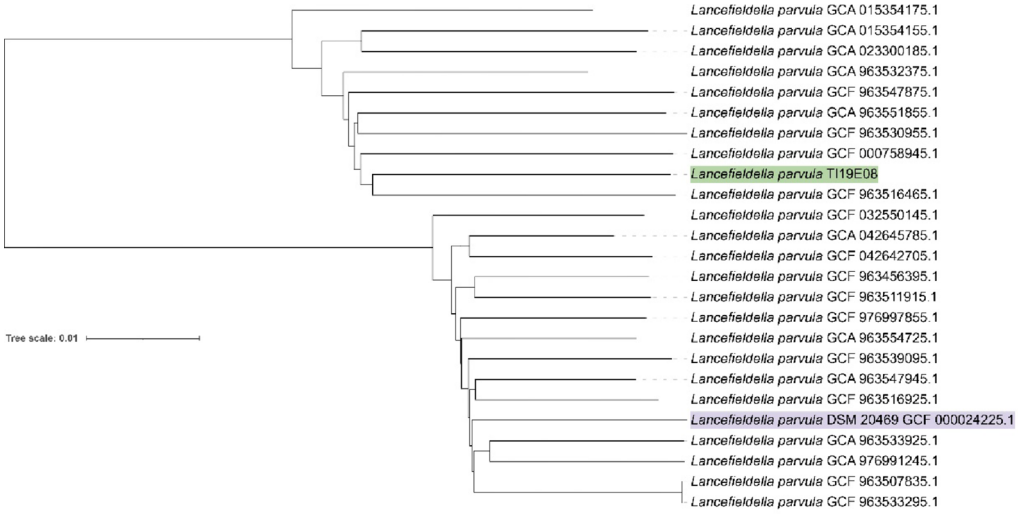


Fig. 1 Phylogenetic analysis of *Lancefieldella parvula* strains. Phylogenetic tree showing the evolutionary relationships among *Lancefieldella parvula* strains, including strain TI19E08 (colored in green) and the type strain DSM 20,469 (colored in purple). Tree inferred with FastME 2.1.6.1 [40] from GBDP distances calculated from genome sequences. The branch lengths are scaled in terms of the GBDP distance formula d_5. The numbers above branches are GBDP pseudobootstrap support values > 60% from 100 replications, with an average branch support of 31.8%. The tree was rooted at the midpoint [41] and visualized via iTOL (version 7.4.2) [32]

while a previously described *L. parvula*-specific primer set (Aparv-711 F/Aparv-881R) [19] and universal bacterial primer set (UniF/R) [33] were used to quantify the total *L. parvula* species and total bacteria, respectively.

The complete genome sequence of *L. parvula* TI19E08 was entered as the template DNA sequence via Primer-BLAST software (https://www.ncbi.nlm.nih.gov/tools/primer-blast/) to design strain specific primers. Parameters were selected to generate primers with melting temperatures (Tm) ranging from 55 to 65 °C and a 70–150 bp product length. The final AtP1F/R primer set showed no predicted amplification from other *Lancefieldella* species and had a final amplicon size of 113 bp. The primer strain specificity was evaluated via PCR using with an *L. parvula* type strain (ATCC 33793), the *L. parvula* TI19E08 isolate, our clinical strain of *L. rimae* and Zymo DNA standards (Zymo Research, Cat.No. D6305. The final AtP1F/R annealing temperature of 66 °C was selected to maintain strain specificity, as lower annealing temperatures resulted in off-target amplification (Supplementary Fig. 2).

Quantitative PCR (qPCR)

Standard curves were generated via serial 10-fold dilutions of both the *L. parvula* type strain (ATCC 33793) and the *L. parvula* TI19E08 isolate's genomic DNA (10^1–10^8 copy number) to determine the detection limit and establish the maximum cycle number (data not shown). The lowest detectable concentrations yield Ct values of 32–33, validating the use of 40 cycles as the maximum threshold.

The quantification of *L. parvula* TI19E08 and total *L. parvula* species relative to total bacteria was performed via a qPCR assay on the extracted metagenomic DNA from MLI samples, using QuantiTect SYBR Green PCR master mix (QIAGEN, 204145) on an Applied Biosystems 7300 DNA analyzer. Each 50 µL reaction mixture contained 25 µL of SYBR Green PCR master mix, 5 µL of template DNA (5 ng/µL), 5 µL of primer mixture (forward and reverse primers, 1 µM final concentration each), and 15 µL of nuclease-free water. The amplification conditions consisted of initial activation at 94 °C for 15 min, followed by 40 cycles of denaturation at 94 °C for 15 s and annealing at 66 °C for 1 min (64 °C for UniF/R primers). All samples were analyzed in triplicate, and data were collected during the annealing step of each cycle.

Cycle threshold (Ct) values were extracted for each sample, and mean Ct values were calculated from technical triplicates. Samples with undetermined Ct values (no amplification with a maximum of 40 cycles) were excluded from the analysis. The relative abundances of the target taxa (*L. parvula* TI19E08 strain and total *L. parvula* species) were calculated using the ΔCt method: ΔCt = target Ct– universal primer Ct. Lower ΔCt values indicate a greater relative abundance of the target taxon relative to the total bacterial load.

Statistical analysis

All the statistical analyses were performed using R (4.2.0). To assess differences in *L. parvula* abundance (ΔCt values) across the inflammatory severity groups, Kruskal–Wallis tests were performed separately for the participants with either UC or CD, and both combined and individual sample locations were analyzed. For significant results ($p < 0.05$), post hoc Dunn's tests with Benjamini–Hochberg correction identified specific group differences. Statistical significance was set at $p < 0.05$ for adjusted p values, with trends identified at adjusted $p < 0.10$.

The relationship between inflammation severity and *L. parvula* relative abundance was evaluated using Spearman correlation analysis. Correlations were calculated separately for the UC and CD using the cor.test function in R, with significance set at $p < 0.05$.

Results

Isolation and genomic characterization of *L. parvula* strain TI19E08

A strain of *Lancefieldella parvula* was isolated from a mucosal luminal interface (MLI) sample collected from the terminal ileum of a participant with UC, using standard microbiology techniques and designated strain TI19E08. Oxford Nanopore long-read sequencing yielded a complete, single contig genome assembly with the assembly statistics summarized in Table 1. The genome is 1,582,852 bp in length with a GC content of 48.17% and 98.9% BUSCO completeness, indicating a high-quality closed assembly.

Whole-genome-based taxonomic analysis was performed using the Type (Strain) Genome Server (TYGS) [31], which employs genome BLAST distance phylogeny (GBDP)-based digital DNA–DNA hybridization (dDDH) for species-level delineation. Whole-genome phylogenomic analysis placed TI19E08 within the *Lancefieldella parvula* clade (Fig. 1), and 16 S rRNA gene-based phylogenetic analysis similarly placed TI19E08 within this clade with a short branch length, closely affiliated with the type strain DSM 20469 and other *L. parvula* strains (Supplementary Fig. 3). The pairwise dDDH values between TI19E08 and the *L. parvula* type strain DSM 20469 was 36.2% (formula d_4), which are below the conventional 70% species boundary threshold; however, similarly, low dDDH values were observed among other confirmed *L. parvula* strain pairs within the TYGS dataset, suggesting that this threshold may not be uniformly applicable across this species.

FastANI [34] analysis revealed 88.8% average nucleotide identity between *L. parvula* TI19E08 and the type strain DSM 20469, which was below the 95% species demarcation cutoff. However, comparison against the closest *L. parvula* genome identified through whole-genome phylogenomic analysis (GCF_963516465.1) yielded 95.37% ANI, exceeding the boundary threshold and confirming species-level affiliation with *L. parvula*. Taken together, the 16 S rRNA phylogenetic placement, whole-genome phylogenomic, and FastANI results collectively support the classification of TI19E08 as a strain of *L. parvula*.

Development and validation of the *L. parvula* TI19E08-specific quantitative PCR assay

To enable precise quantification of the clinical isolate in complex microbiome samples, strain-specific primers (AtP1F/R) were designed using NCBI Primer-BLAST to target unique genomic regions in TI19E08. We validated that the AtP1F/R primer set exclusively amplified DNA from *L. parvula* TI19E08, with no amplification against the *L. parvula*-type strain or a *Lancefieldella rimae* clinical strain isolated from the same participant under our qPCR assay conditions (Supplementary Fig. 2).

L. parvula TI19E08 abundance is correlated with inflammation severity in UC

Quantitative PCR analysis revealed significant associations between *L. parvula* TI19E08 relative abundance and inflammation severity in participants with UC. Given that the terminal ileum (TI) was uniformly uninvolved in our UC participants, this region was excluded from analysis in this group. We first assessed TI19E08 associations with disease severity in UC by merging samples with the same Mayo score. This revealed significant overall differences between inflammation severity grades ($p < 0.05$, Fig. 2A). Post hoc pairwise comparisons revealed a stepwise increase in bacterial abundance with increasing inflammation severity, with severe inflammation (grade 3) resulting in significantly greater *L. parvula* TI19E08 levels than both normal/inactive disease (grade 0 vs. grade 3, $p < 0.05$) and mild inflammation (grade 1 vs. grade 3, $p < 0.01$). Additionally, moderate inflammation significantly elevated *L. parvula* TI19E08 abundance compared with mild inflammation (grade 1 vs. grade 2, $p < 0.05$), indicating a progressive relationship between the *L. parvula* TI19E08 load and inflammation severity. Spearman correlation analysis confirmed a significant negative correlation between inflammation grade and *L. parvula* TI19E08 abundance across UC samples (Spearman $\rho = -0.58$ & $p < 0.05$) (Fig. 2C).

We next conducted an anatomical location-specific analysis and this revealed distinct colonization patterns within the colon (Fig. 2B). In the proximal colon, *L. parvula* TI19E08 exhibited significant differences across inflammation grades, with both moderate and severe inflammation displaying significantly greater abundances than both normal/inactive disease (grade 0 vs. grade 2, $p < 0.05$; grade 0 vs. grade 3, $p < 0.05$) and mild inflammation (grade 1 vs. grade 2, $p < 0.05$; grade 1 vs. grade 3, $p < 0.05$). No significant differences were observed between the moderate and severe inflammation grades ($p = 0.40$). In the distal colon, although overall statistical significance was not achieved between the inflammation grade pairs ($p = 0.08$), notable trends toward significance emerged for severe inflammation (grade 3), which was associated with greater *L. parvula* TI19E08 abundance than normal/inactive disease (grade 0) (p adj = 0.05) and moderate inflammation (grade 2) (p adj = 0.06), which is consistent with the overall pattern of inflammation-associated *L. parvula* TI19E08 enrichment.

Total *L. parvula* species abundance is correlated with inflammation severity in UC

Analysis of total *L. parvula* species abundance in UC microbiomes revealed similar inflammation-associated patterns as *L. parvula* TI19E08, with significant overall differences across inflammation grades (Fig. 3A). Post hoc analysis revealed that severe inflammation resulted in significantly greater total *L. parvula* abundance than both normal/inactive disease (grade 0 vs. grade 3, $p < 0.01$) and moderate inflammation (grade 2 vs. grade 3, $p < 0.05$), indicating that inflammation-associated enrichment extends beyond the specific clinical isolate to encompass the broader *L. parvula* population. Spearman correlation analysis confirmed a significant negative correlation between inflammation grade and total *L. parvula* abundance across UC samples (Spearman $\rho = -0.43$ & $p < 0.05$) (Fig. 3C).

Regional analysis revealed anatomically distinct patterns of total *L. parvula* distribution across inflammation severities (Fig. 3B). In the proximal colon, significant differences were observed across inflammation grades, with mild, moderate and severe inflammation, all of which significantly elevated bacterial abundance relative to that of inactive/normal disease (grade 0 vs. grades 1 and 3; $p < 0.01$, grade 0 vs. grade 2; $p < 0.05$), suggesting that any degree of inflammatory activity promotes *L. parvula* colonization in this anatomical region. In contrast, distal colon locations showed no statistically significant differences across inflammation grades ($p = 0.10$), although they tended toward greater abundance in severe inflammation than in moderate inflammation (grade 3 vs. grade 2, $p = 0.053$) and mild inflammation (grade 3 vs. grade 1, $p = 0.092$), which is consistent with the strain-specific patterns observed for *L. parvula* TI19E08.

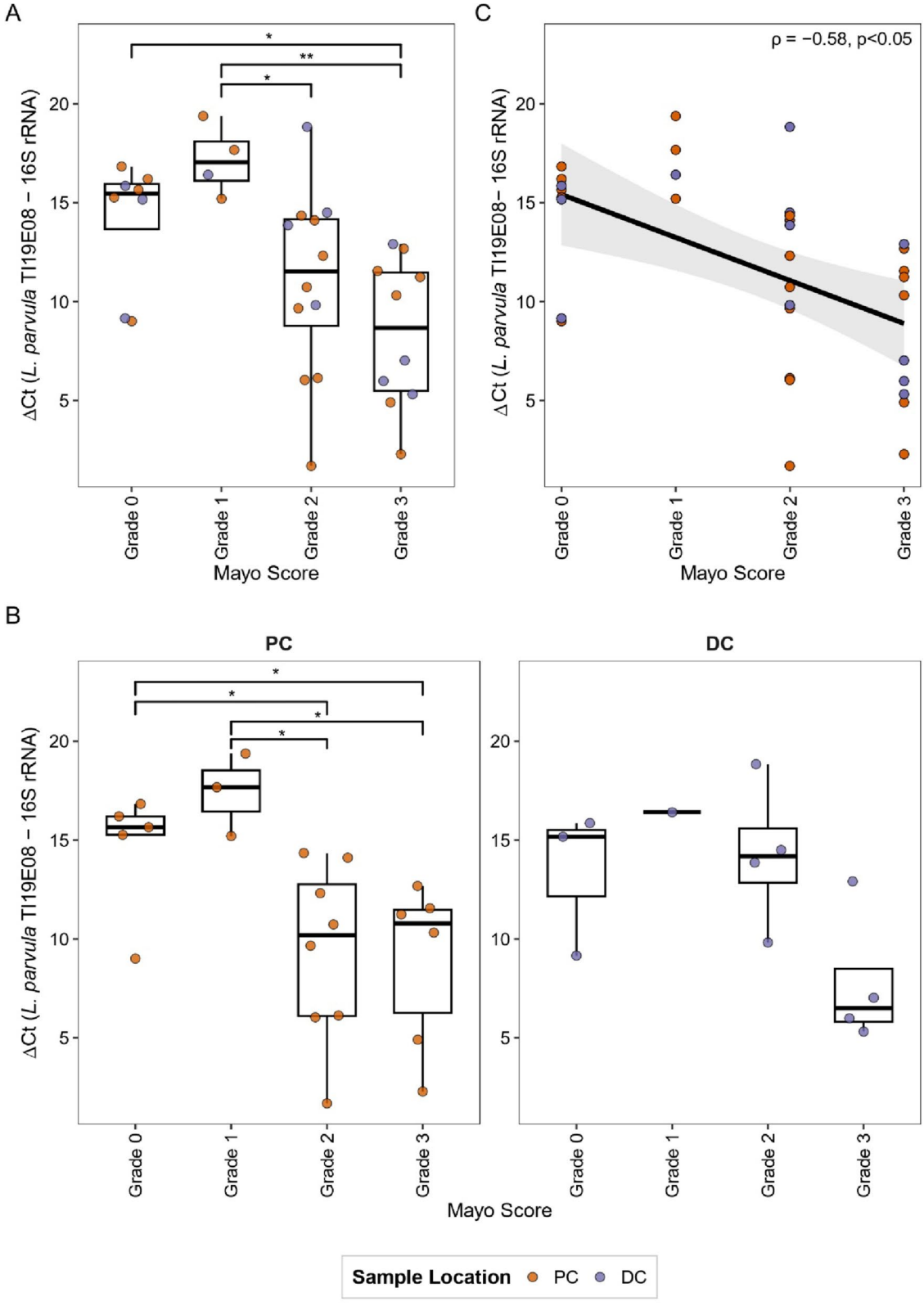


Fig. 2 qPCR quantification of *L. parvula* TI19E08 in the UC microbiome as a function of inflammation severity. Each point shows ΔCt values, colored by sample location; PC = proximal colon, DC = distal colon. (**A**) PC and DC samples are combined. (**B**) Location-specific analysis showing PC and DC samples separately. Statistical comparisons were performed using the Kruskal–Wallis test followed by Dunn's post hoc test with Benjamini–Hochberg (BH) correction. Significance levels are indicated as follows: * $p < 0.05$, ** $p < 0.01$. (**C**) Spearman correlation between *L. parvula* TI19E08 relative abundance and UC inflammation severity ($\rho = -0.58$, $p < 0.05$)

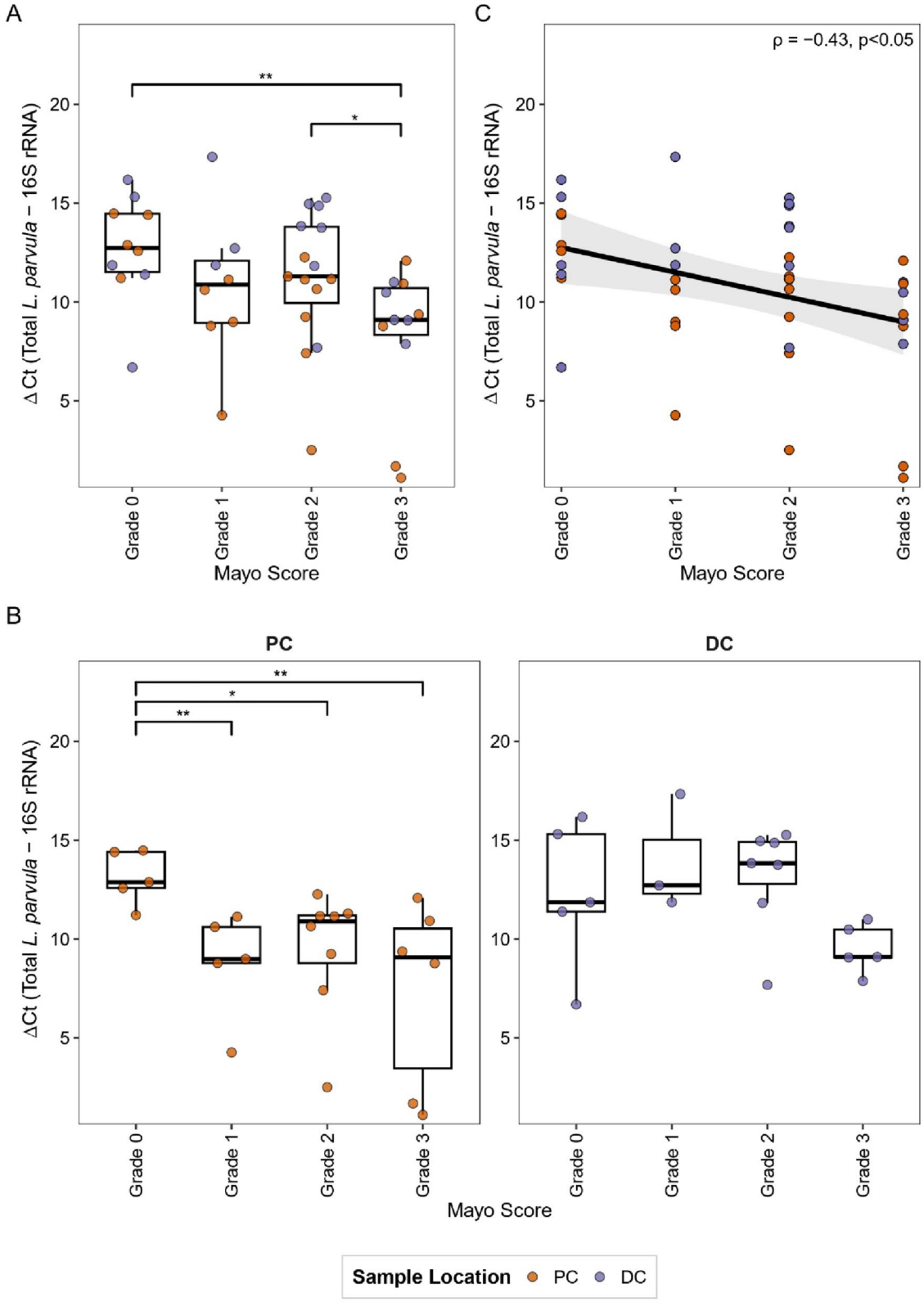


Fig. 3 qPCR quantification of total *L. parvula* in the UC microbiome as a function of inflammation severity. Each point shows ΔCt values, colored by sample location; PC = proximal colon, DC = distal colon. (**A**) PC and DC samples are combined. (**B**) Location-specific analysis showing PC and DC samples separately. Statistical comparisons were performed using the Kruskal–Wallis test followed by Dunn's post hoc test with Benjamini–Hochberg (BH) correction. Significance levels are indicated as follows: * $p < 0.05$, ** $p < 0.01$. (**C**) Spearman correlation between total *L. parvula* relative abundance and UC inflammation severity ($\rho = -0.43$, $p < 0.05$)

L. parvula TI19E08 abundance is correlated with inflammation severity in CD

In CD participants, analysis using all anatomical locations revealed no significant overall differences in *L. parvula* TI19E08 abundance across inflammation severity groups (p adj = 0.11, Fig. 4A), reflecting the heterogeneous nature of CD pathology. However, Spearman correlation analysis confirmed a significant negative correlation between inflammation grade and *L. parvula* TI19E08 abundance across CD samples (Spearman ρ = −0.37 & $p < 0.05$) (Fig. 4C). Anatomical location-specific analysis revealed significant associations in disease-related regions (Fig. 4B). The terminal ileum, a primary site of CD involvement, demonstrated significant overall differences across SES-CD score groups. Post hoc analysis revealed that inflammation with increased scores (SES-CD score 7–9) was associated with significantly greater *L. parvula* TI19E08 abundance than was lower SES-CD score (SES-CD score 0, $p < 0.05$; SES-CD score 4–6, $p < 0.05$). Similarly, a higher inflammation score (SES-CD score 10–12) was associated with significantly greater bacterial abundance than a lower inflammation score (SES-CD score 4–6, $p < 0.05$), with a trend toward greater abundance than inactive disease (SES-CD score 0, $p = 0.08$).

Neither proximal nor distal colon locations demonstrated significant differences in *L. parvula* TI19E08 abundance across inflammation severity scores ($p = 0.56$ and $p = 0.16$ respectively), although the distal colon presented a trend toward higher *L. parvula* TI19E08 abundance in individuals with higher inflammation scores (SES-CD scores of 7–9) than in those with lower scores (SES-CD scores of 1–3, $p = 0.07$).

Total *L. parvula* species abundance is correlated with inflammation severity in CD

Analysis of *L. parvula* abundance in CD revealed more modest associations with inflammation severity than in UC. Across all the anatomical locations, no significant differences were observed across the inflammation severity groups ($p = 0.14$) (Fig. 5A), with a trend toward an increase in the SES-CD score of 7–9 compared with the SES-CD score of 1–3 (p adj = 0.09). Anatomical location-specific analysis revealed that neither the terminal ileum nor the proximal colon demonstrated significant differences across inflammation severity scores ($p = 0.53$ and $p = 0.47$ respectively) (Fig. 5B). However, the distal colon exhibited significant overall differences in inflammation severity scores, with a higher inflammation score (SES-CD score of 7–9) indicating significantly greater total *L. parvula* abundance than lower inflammation scores (SES-CD score of 1–3, $p < 0.05$) and a trend toward greater abundance than SES-CD score of 4–6 (p adj = 0.08).

Discussion

Our findings demonstrate that *L. parvula* abundance correlates with inflammation severity in IBD, with distinct disease-specific and anatomically specific patterns that provide new insight into the ecological role of this emerging pathobiont in IBD pathogenesis. The development of a strain-specific quantitative PCR assay enabled precise discrimination between the clinical isolate TI19E08 and other *L. parvula* strains, revealing that both strain-specific and species-level abundance patterns are associated with inflammation severity.

These findings extend our previous work in which we reported enrichment of *Lancefieldella* (*Atopobium*) *parvula* at the proximal colon mucosal–luminal interface in pediatric patients with Crohn's disease [19], with the ATCC type strain used as a reference. In that study, *L. parvula* was identified as part of an inflammation-associated microbial signature localized to the host–microbe interface. The present study advances those observations by demonstrating that a clinical intestinal isolate (TI19E08) quantitatively tracks graded endoscopic inflammation severity and does so across IBD subtypes and anatomical regions.

In UC, both *L. parvula* strain TI19E08 and total *L. parvula* spp. presented clear positive correlations with inflammation severity, with the strongest associations observed in moderate to severe inflammation compared with normal/inactive or mild disease. This stepwise/dose−response relationship suggests that *L. parvula* colonization is not merely a binary response to inflammatory conditions but rather scales proportionally with the degree of tissue inflammation. These findings raise the possibility that clinical strains of *L. parvula* could serve as a potential quantitative correlate of inflammatory activity in UC, where current diagnostic approaches rely primarily on endoscopic and histological assessments that may not capture the full spectrum of subclinical inflammatory variation [35, 36].

L. parvula colonization patterns in UC reflect anatomical differences in inflammatory environments, with the proximal colon showing the strongest strain-specific association across all inflammation grades, whereas the distal colon presents more selective species-level enrichment. These region-specific differences suggest that *L. parvula* strains may occupy distinct ecological niches within the inflamed colon, with proximal colon colonization serving as a particularly sensitive indicator of inflammatory activity that may precede clinically apparent tissue damage.

The relationship between *L. parvula* and inflammation in CD patients is complex, reflecting the heterogeneous and discontinuous nature of CD pathology [37] and the regional sampling characteristics of MLI aspirate samples. Unlike UC, where continuous mucosal

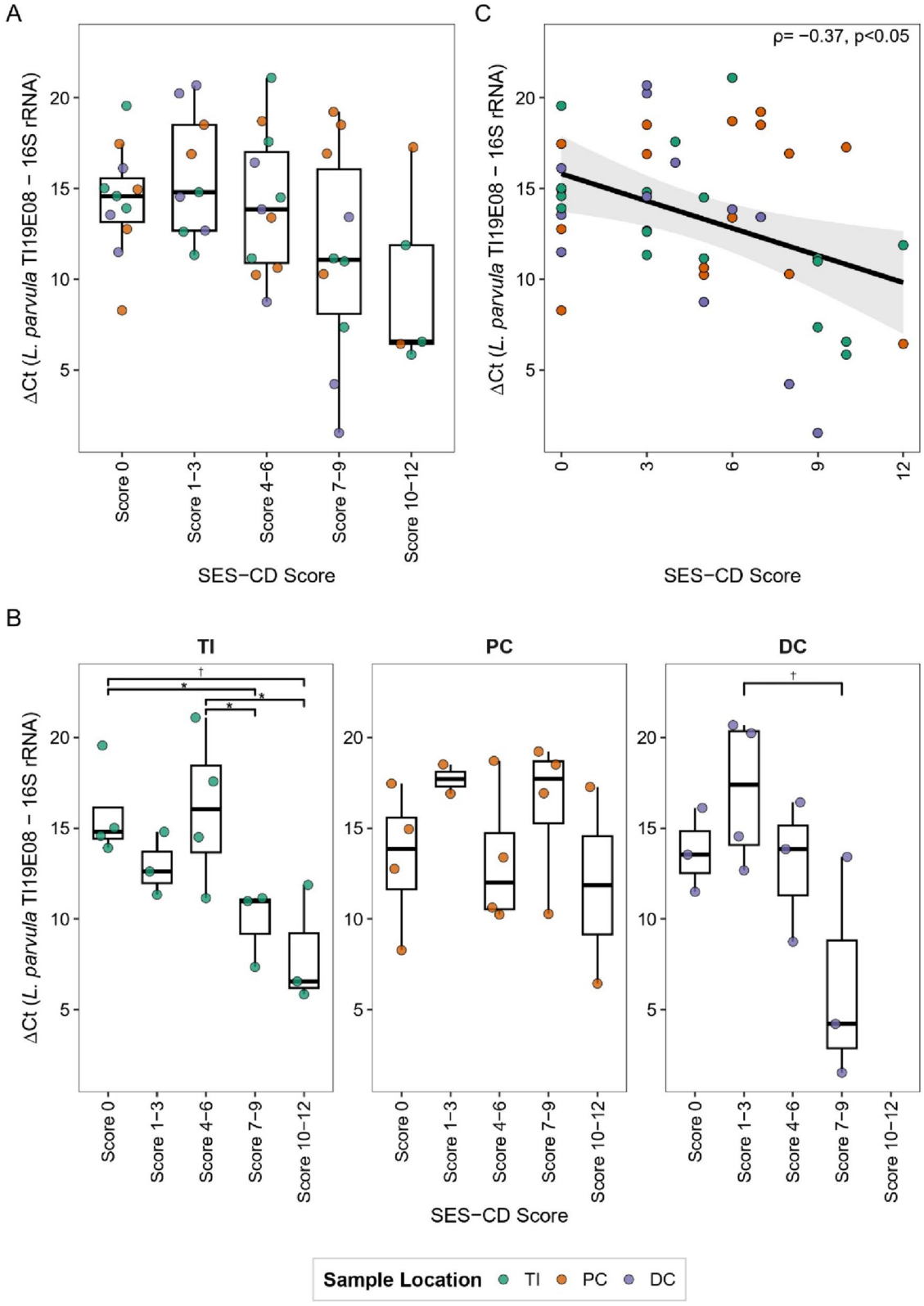


Fig. 4 qPCR quantification of *L. parvula* TI19E08 in the CD microbiome as a function of inflammation severity. Each point shows ΔCt values, colored by sample location; TI = terminal ileum, PC = proximal colon, DC = distal colon. (**A**) TI, PC and DC locations are combined. (**B**) Location-specific analysis showing TI, PC and DC samples separately. Statistical comparisons were performed using the Kruskal–Wallis test followed by Dunn's post hoc test with Benjamini–Hochberg (BH) correction. Significance levels are indicated as follows: * $p < 0.05$, ** $p < 0.01$, † $p < 0.10$. (**C**) Spearman correlation between *L. parvula* TI19E08 relative abundance and CD inflammation severity ($\rho = -0.37$, $p < 0.05$)

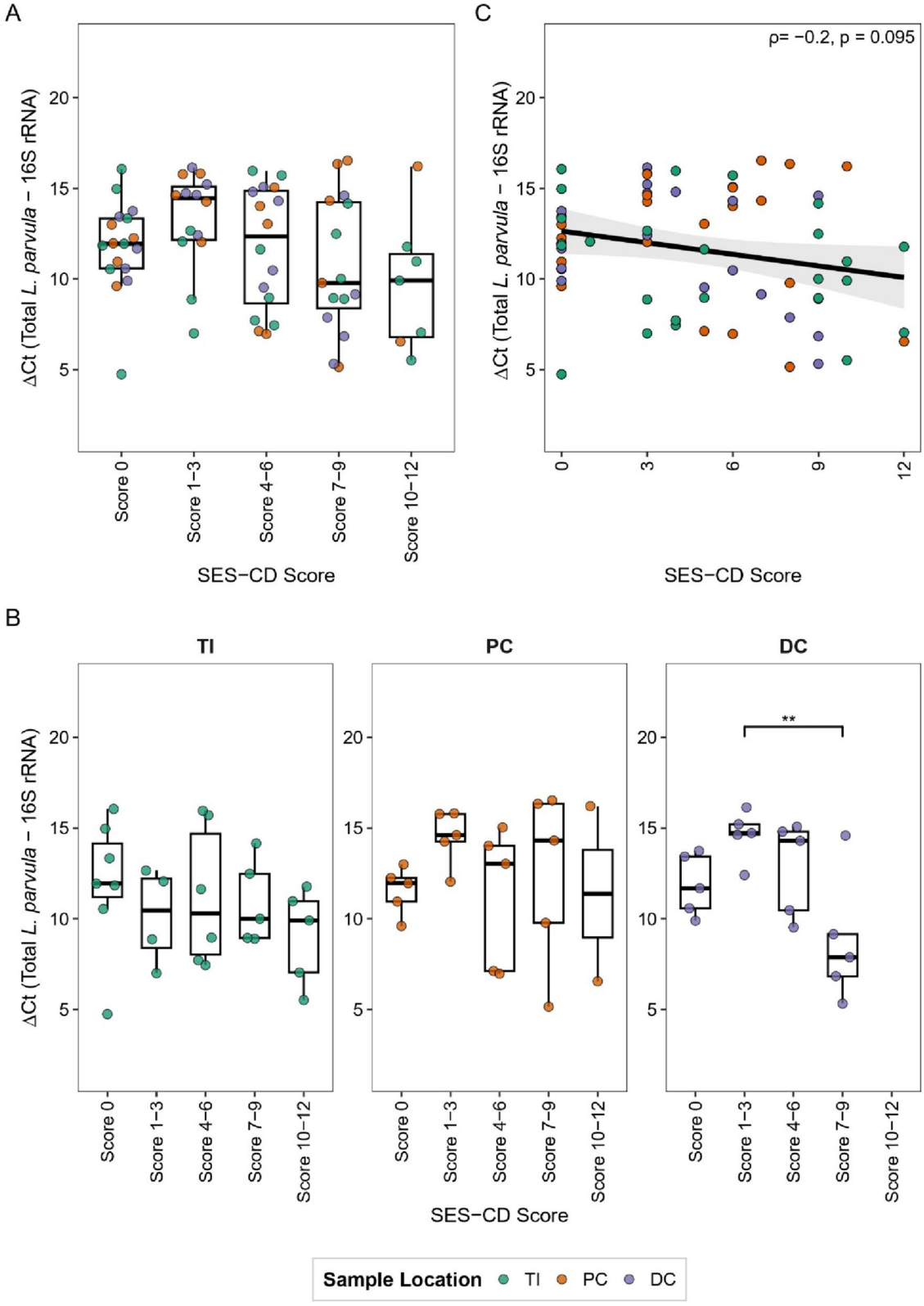


Fig. 5 qPCR quantification of total *L. parvula* in the CD microbiome as a function of inflammation severity. Each point shows delta Ct values, colored by sample location; TI = terminal ileum, PC = proximal colon, DC = distal colon. (**A**) TI, PC and DC samples are combined. (**B**) Location-specific analysis showing TI, PC and DC samples separately. Statistical comparisons were performed using the Kruskal–Wallis test followed by Dunn's post hoc test with Benjamini–Hochberg (BH) correction. Significance levels are indicated as follows: * $p < 0.05$, ** $p < 0.01$. (**C**) Spearman correlation between total *L. parvula* relative abundance and CD inflammation severity ($\rho = -0.20$, $p = 0.095$)

involvement yields specimens from uniformly inflamed or non-inflamed mucosa, CD aspirates would include both; potentially attenuating *L. parvula* abundance signals and may be contributing to the weaker associations observed in this group. In addition, *L. parvula* TI19E08 was significantly associated with inflammation severity, whereas total *L. parvula* levels presented weaker associations, highlighting the importance of strain-level analysis in CD. Location-specific analysis revealed that the terminal ileum, a primary site of CD involvement [38, 39], had the strongest associations with *L. parvula* TI19E08 abundance and inflammation severity. Notably, TI19E08 was itself isolated from the terminal ileum, raising the possibility that this strain is particularly adapted to the terminal ileum. This site-specific pattern aligns with the characteristic disease distribution of CD and suggests that *L. parvula* expansion requires the specific inflammatory microenvironment present at sites of active disease involvement.

On the basis of our data, the increased abundance of *L. parvula* in inflamed tissue raises fundamental questions about causality. Our correlative data supports nonmutually exclusive possibilities *L. parvula* may act as an early colonizer that shapes the gut environment and promotes the expansion of pathogenic taxa, may expand in response to inflammation and subsequently exacerbate disease severity, or may primarily represent a consequence of inflammation without a direct causal role. This latter possibility is supported by the organism's in vitro growth requirement for serum supplementation, which may be recapitulated in vivo by inflammation-associated protein losing enteropathy. The observed dose–response relationship supports multiple interpretations, as progressive inflammatory activity could either result from increasing pathobiont burden or reflect increasingly favorable conditions for bacterial expansion.

Importantly, in our prior study using an IBD-susceptible gnotobiotic mouse model, we demonstrated that *Lancefieldella (Atopobium) parvula* induces severe pancolitis in a microbiota-dependent manner, as monoassociated mice did not develop colitis [19]. Those experiments were conducted using the ATCC-type strain originally isolated from the oral cavity, whereas the present study focused on a clinical intestinal isolate (TI19E08). Although genomic heterogeneity exists within the species, the prior demonstration of proinflammatory potential together with the inflammation-associated expansion observed here suggests that *L. parvula* may contribute to disease pathogenesis rather than simply reflecting inflammatory conditions.

Our findings provide the first quantitative assessment of *L. parvula* inflammation-associated abundance patterns across IBD subtypes and anatomical regions. While previous work identified associations only in pediatric CD [19], we demonstrated inflammation-correlated patterns in both CD and UC. These discoveries extend the characterization of *L. parvula* across the broader IBD spectrum and suggest that therapeutic strategies must consider strain-level variation in pathogenic potential. However, several limitations must be acknowledged. The cross-sectional study design precludes the determination of causality in the relationship between *L. parvula* abundance and inflammation severity. Additionally, our analysis focused on a single clinical isolate, and the generalizability of strain-specific findings to other *L. parvula* present in IBD populations remains unclear. Moreover, the small sample size resulted in limited statistical power for some inflammation severity comparisons, indicating validation in larger cohorts with sufficient representation across the full spectrum of inflammation activity.

Conclusions

The study provides initial evidence for the clinical relevance of an intestinal *L. parvula* isolate (TI19E08) in IBD and demonstrates that strain-level expansion correlates with endoscopic inflammation severity across both UC and CD subtypes and anatomical regions. The strong correlation between *L. parvula* TI19E08 abundance and inflammation severity identifies this strain as candidate marker warranting validation in larger, particularly in UC. Future research should focus on mechanistic characterization, longitudinal validation and exploration of targeted therapeutic strategies to potentially modulate the *L. parvula* TI19E08 population in IBD.

Abbreviations

ANI	Average nucleotide identity
CD	Crohn's disease
DC	Distal colon
dDDH	Digital DNA-DNA hybridization
IBD	Inflammatory bowel disease
MLI	Mucosal luminal interface
OD	Optical density
PC	Proximal colon
PCDAI	Pediatric Crohn's disease activity index
PUCAI	Pediatric ulcerative colitis activity index
qPCR	Quantitative polymerase chain reaction
SES-CD	Simple endoscopic score for Crohn's disease
TI	Terminal ileum
UC	Ulcerative colitis

Supplementary Information

The online version contains supplementary material available at https://doi.org/10.1186/s13099-026-00865-x.

Supplementary Material 1: Growth curve of *L. parvula* TI19E08. The growth of *L. parvula* TI19E08 was monitored over 21 hours by measuring the optical density at 600 nm. The culture reached the maximum optical density at approximately 4 hours, followed by a slight decrease before stabilizing, indicative of a transition from the exponential phase to the stationary phase

Supplementary Material 2: Analysis of AtP1F/R primers specificity at different annealing temperatures. PCR products from various bacterial strains and primer sets were visualized on agarose gels. AtP1F/R was tested at annealing temperatures of 64 °C (A) and 66 °C (B). There was faint-off

target amplicon of the *L. parvula* type strain at 64 °C (A) but no amplification seen for *L. rimae* TI19B36. Increasing the annealing temperature to 66 °C eliminated this off-target amplification (B) and thus 66 °C was used for the final assay conditions

Supplementary Material 3: Phylogenetic analysis of *Lancefieldella parvula* strains. Phylogenetic tree showing the evolutionary relationships among *Lancefieldella parvula* strains, including strain TI19E08 (colored in green) and the type strain DSM 20469 (colored in purple). Tree inferred with FastME 2.1.6.1 [40] from GBDP distances calculated from 16S rDNA gene sequences. The branch lengths are scaled in terms of the GBDP distance formula d5. The numbers above branches are GBDP pseudobootstrap support values > 60% from 100 replications, with an average branch support of 64.3%. The tree was rooted at the midpoint41 and visualized using iTOL (version 7.4.2) [32

Acknowledgements
We thank Ruth Singleton for her expertise in participant recruitment and sample and data collection. This research was enabled in part by the Digital Research Alliance of Canada (alliancecan.ca).

Author contributions
SW performed the qPCR assays, whole genome sequencing and primary data analysis, and wrote the initial manuscript draft. AY isolated ***L. parvula*** TI19E08 from a participant and performed short-read sequencing. SW and AS jointly designed the experiments. DRM was responsible for sample collection and clinical data generation and interpretation. JB provided guidance on data interpretation. All authors reviewed and approved the final manuscript.

Funding
This work was funded by the Government of Canada through Genome Canada and the Ontario Genomics Institute (OGI-149), the Canadian Institutes of Health Research (ECD-144627), the Ontario Ministry of Economic Development and Innovation (Project 13440), and the Weston Family Foundation.

Data availability
The Lancefiedella parvula TI19E08 genome assembly and raw sequencing data generated during this study are available in NCBI under BioProject accession PRJNA1428198.

Declarations

Ethics approval and consent to participate
The collection of samples from pediatric IBD participants was approved by the Research Ethics Board of the Children's Hospital of Eastern Ontario (CHEO, #09/37X) in Ottawa, Canada. Informed written consent/assent was obtained from parents and/or participants prior to sample collection.

Consent for publication
Not applicable.

Competing interests
AS and DRM are co-founders of MedBiome, a clinical microbiomics company. The other authors have no competing interests to declare.

Received: 11 May 2026 / Accepted: 24 July 2026
Published online: 14 August 2026

References

1. Wang R, Li Z, Liu S, Zhang D. Global, regional and national burden of inflammatory bowel disease in 204 countries and territories from 1990 to 2019: a systematic analysis based on the Global Burden of Disease Study 2019. BMJ Open. 2023;13(3):e065186. https://doi.org/10.1136/bmjopen-2022-065186.
2. Xavier RJ, Podolsky DK. Unravelling the pathogenesis of inflammatory bowel disease. Nature. 2007;448(7152):427–34. https://doi.org/10.1038/nature06005 .
3. Greenstein AJ, Janowitz HD, Sachar DB. The extra-intestinal complications of Crohn's disease and ulcerative colitis: a study of 700 patients. Medicine (Baltimore). 1976;55(5):401–12. https://doi.org/10.1097/00005792-197609000-00004.
4. Torres J, Mehandru S, Colombel JF, Peyrin-Biroulet L. Crohn's disease. Lancet. 2017;389(10080):1741–55. https://doi.org/10.1016/S0140-6736(16)31711-1.
5. Ordás I, Eckmann L, Talamini M, Baumgart DC, Sandborn WJ. Ulcerative colitis. Lancet. 2012;380(9853):1606–19. https://doi.org/10.1016/S0140-6736(12)60150-0.
6. Hyams JS, Ferry GD, Mandel FS, Gryboski JD, Kibort PM, Kirschner BS, et al. Development and Validation of a Pediatric Crohn's Disease Activity Index. J Pediatr Gastroenterol Nutr. 1991;12(4):439. https://doi.org/10.1097/00005176-199105000-00005.
7. Turner D, Levine A, Walters TD, Focht G, Otley A, López VN, et al. Which PCDAI version best reflects intestinal inflammation in pediatric Crohn disease? J Pediatr Gastroenterol Nutr. 2017;64(2):254–60. https://doi.org/10.1097/MPG.0000000000001227.
8. Turner D, Otley AR, Mack D, Hyams J, De Bruijne J, Uusoue K, et al. Development, validation, and evaluation of a pediatric ulcerative colitis activity index: a prospective multicenter study. Gastroenterology. 2007;133(2):423–32. https://doi.org/10.1053/j.gastro.2007.05.029.
9. Copeland A, Sikorski J, Lapidus A, Nolan M, Del Rio TG, Lucas S, et al. Complete genome sequence of *Atopobium parvulum* type strain (IPP 1246T). Stand Genomic Sci. 2009;1(2):166–73. https://doi.org/10.4056/sigs.29547.
10. Verma D, Garg PK, Dubey AK. Insights into the human oral microbiome. Arch Microbiol. 2018;200(4):525–40. https://doi.org/10.1007/s00203-018-1505-3.
11. Nardelli C, Granata I, D'argenio V, Tramontano S, Compare D, Guarracino MR, et al. Characterization of the duodenal mucosal microbiome in obese adult subjects by 16s rrna sequencing. Microorganisms. 2020;8(4):1–13. https://doi.org/10.3390/microorganisms8040485.
12. Harmsen HJM, Wildeboer-Veloo ACM, Grijpstra J, Knol J, Degener JE, Welling GW. Development of 16S rRNA-based probes for the Coriobacterium group and the Atopobium cluster and their application for enumeration of Coriobacteriaceae in human feces from volunteers of different age groups. Appl Environ Microbiol. 2000;66(10):4523–7. https://doi.org/10.1128/AEM.66.10.4523-4527. 2000 PubMed PMID: 11010909.
13. Kho ZY, Lal SK. The human gut microbiome - A potential controller of wellness and disease. Front Microbiol. 2018;9(AUG):1–23. https://doi.org/10.3389/fmicb.2018.01835 . PubMed PMID: 30154767.
14. Kazor CE, Mitchell PM, Lee AM, Stokes LN, Loesche WJ, Dewhirst FE, et al. Diversity of bacterial populations on the tongue dorsa of patients with halitosis and healthy patients. J Clin Microbiol. 2003;41(2):558–63. https://doi.org/10.1128/JCM.41.2.558-563.2003.
15. Yachida S, Mizutani S, Shiroma H, Shiba S, Nakajima T, Sakamoto T, et al. Metagenomic and metabolomic analyses reveal distinct stage-specific phenotypes of the gut microbiota in colorectal cancer. Nat Med. 2019;25(6):968–76. https://doi.org/10.1038/s41591-019-0458-7 . PubMed PMID: 31171880.
16. Mizutani S, Yamada T, Yachida S. Significance of the gut microbiome in multistep colorectal carcinogenesis. Cancer Sci. 2020;111(3):766–73. https://doi.org/10.1111/cas.14298 . PubMed PMID: 31910311.
17. Narii N, Zha L, Sobue T, Kitamura T, Komatsu M, Shimomura Y, et al. Intestinal Bacteria Fluctuating in Early-Stage Colorectal Cancer Carcinogenesis are Associated with Diet in Healthy Adults. Nutr Cancer. 2024;76(6):521–8. https://doi.org/10.1080/01635581.2024.2344257 . PubMed PMID: 38642022.
18. Maarsingh JD, Łaniewski P, Herbst-Kralovetz MM. Immunometabolic and potential tumor-promoting changes in 3D cervical cell models infected with bacterial vaginosis-associated bacteria. Commun Biol. 2022;5(1):1–13. https://doi.org/10.1038/s42003-022-03681-6 . PubMed PMID: 35869172.
19. Mottawea W, Chiang CK, Mühlbauer M, Starr AE, Butcher J, Abujamel T, et al. Altered intestinal microbiota–host mitochondria crosstalk in new onset Crohn's disease. Nat Commun. 2016;7(1):13419. https://doi.org/10.1038/ncomms13419.
20. Kumbhari A, Cheng TNH, Ananthakrishnan AN, Kochar B, Burke KE, Shannon K, et al. Discovery of disease-adapted bacterial lineages in inflammatory bowel diseases. Cell Host Microbe. 2024;32(7):1147–e116212. https://doi.org/10.1016/j.chom.2024.05.022.
21. Mottawea W, Butcher J, Li J, Abujamel T, Manoogian J, Mack D, et al. The mucosal–luminal interface: an ideal sample to study the mucosa-associated microbiota and the intestinal microbial biogeography. Pediatr Res. 2019;85(6):895–903. https://doi.org/10.1038/s41390-019-0326-7 . PubMed PMID: 30758325.

22. Schroeder KW, Tremaine WJ, Ilstrup DM. Coated oral 5-aminosalicylic acid therapy for mildly to moderately active ulcerative colitis. N Engl J Med. 1987;317(26):1625–9. https://doi.org/10.1056/NEJM198712243172603.
23. Daperno M, D'Haens G, Van Assche G, Baert F, Bulois P, Maunoury V, et al. Development and validation of a new, simplified endoscopic activity score for Crohn's disease: the SES-CD. Gastrointest Endosc. 2004;60(4):505–12. https://doi.org/10.1016/S0016-5107(04)01878-4.
24. Liu D. Molecular Detection of Human Bacterial Pathogens. In. CRC Press; 2011. p. 31 of 1278.
25. Van Belkum A, Hermans PWM. BOX PCR Fingerprinting for Molecular Typing of Streptococcus pneumoniae. In: Antibiotic Resistance Methods and Protocols. New Jersey: Humana Press; 2000. p. 159–68. https://doi.org/10.1385/1-59259-077-2:159.
26. Kolmogorov M, Yuan J, Lin Y, Pevzner PA. Assembly of long, error-prone reads using repeat graphs. Nat Biotechnol. 2019;37(5):540–6. https://doi.org/10.1038/s41587-019-0072-8.
27. Li H. Aligning sequence reads, clone sequences and assembly contigs with BWA-MEM [Internet]. arXiv; 2013 [cited 2026 Feb 23]. Available from: https://arxiv.org/abs/1303.3997 https://doi.org/10.48550/ARXIV.1303.3997
28. Wick RR, Holt KE. Polypolish: short-read polishing of long-read bacterial genome assemblies. PLoS Comput Biol. 2022;18(1):e1009802. https://doi.org/10.1371/journal.pcbi.1009802.
29. Gurevich A, Saveliev V, Vyahhi N, Tesler G. QUAST: quality assessment tool for genome assemblies. Bioinformatics. 2013;29(8):1072–5. https://doi.org/10.1093/bioinformatics/btt086.
30. Manni M, Berkeley MR, Seppey M, Simão FA, Zdobnov EM. BUSCO update: novel and streamlined workflows along with broader and deeper phylogenetic coverage for scoring of eukaryotic, prokaryotic, and viral genomes. Mol Biol Evol. 2021;38(10):4647–54. https://doi.org/10.1093/molbev/msab199.
31. Meier-Kolthoff JP, Göker M. TYGS is an automated high-throughput platform for state-of-the-art genome-based taxonomy. Nat Commun. 2019;10(1):2182. https://doi.org/10.1038/s41467-019-10210-3.
32. Letunic I, Bork P. Interactive tree of life (iTOL) v6: recent updates to the phylogenetic tree display and annotation tool. Nucleic Acids Res. 2024;52(W1):W78-82. https://doi.org/10.1093/nar/gkae268.
33. Fuller Z, Louis P, Mihajlovski A, Rungapamestry V, Ratcliffe B, Duncan AJ. Influence of cabbage processing methods and prebiotic manipulationof colonic microflora on glucosinolate breakdown in man. Br J Nutr. 2007;98(2):364–72. https://doi.org/10.1017/S0007114507709091.
34. Jain C, Rodriguez-R LM, Phillippy AM, Konstantinidis KT, Aluru S. High throughput ANI analysis of 90K prokaryotic genomes reveals clear species boundaries. Nat Commun. 2018;9(1):5114. https://doi.org/10.1038/s41467-018-07641-9.
35. Pai RK, Jairath V, Vande Casteele N, Rieder F, Parker CE, Lauwers GY. The emerging role of histologic disease activity assessment in ulcerative colitis. Gastrointest Endosc. 2018;88(6):887–98. https://doi.org/10.1016/j.gie.2018.08.018.
36. George A, Gottlieb K, Baxi S, Eastman W, Colucci D, Battioui C, et al. P0264 Using a machine learning model to grade clip-level endoscopic inflammation reveals the heterogeneity of mucosal inflammation in ulcerative colitis. J Crohns Colitis. 2025;19(Supplement1):i697–8. https://doi.org/10.1093/ecco-jcc/jjae190.0438.
37. Fang HM. Intricacy of Crohn's disease: incongruity between diagnostic modalities and histopathologic assessment. World J Gastrointest Endosc. 2025. https://doi.org/10.4253/wjge.v17.i4.103979.
38. Caprilli R. Why does Crohn's disease usually occur in terminal ileum? J Crohns Colitis. 2008;2(4):352–6. https://doi.org/10.1016/j.crohns.2008.06.001.
39. Goulart RDA, Barbalho SM, Gasparini RG, De Carvalho ADCA. Facing Terminal Ileitis: Going Beyond Crohn's Disease. Gastroenterol Res. 2016;9(1):1–9. https://doi.org/10.14740/gr698w.
40. Lefort V, Desper R, Gascuel O. FastME 2.0: a comprehensive, accurate, and fast distance-based phylogeny inference program: Table 1. Mol Biol Evol. 2015;32(10):2798–800. https://doi.org/10.1093/molbev/msv150.
41. Farris JS. Estimating Phylogenetic Trees from Distance Matrices. Am Nat. 1972;106(951):645–68. https://doi.org/10.1086/282802.
42. Edwards U, Rogall T, Blöcker H, Emde M, Böttger EC. Isolation and direct complete nucleotide determination of entire genes. Characterization of a gene coding for 16S ribosomal RNA. Nucleic Acids Res. 1989;17(19):7843–53. https://doi.org/10.1093/nar/17.19.7843.

Publisher's note

Springer Nature remains neutral with regard to jurisdictional claims in published maps and institutional affiliations.